# Negative Effective Mass Mechanism of Negative Differential Drift Velocity and Terahertz Generation

Zinovi S. Gribnikov, Rustam R. Bashirov, and Vladimir V. Mitin, *Senior Member, IEEE*

***Abstract*—The negative-differential-drift-velocity instability, which forms the basis of Gunn high-frequency generators, can originate from Ridley–Watkins–Hilsum or negative effective mass (NEM) mechanisms. The first mechanism is dissipative by nature. The second is mainly drift-related. Therefore, the second mechanism promises to be more effective. We show the existence of stationary oscillatory regimes in the ballistic NEM $p^+pp^+$-diodes, which have a base in the form of a periodic system of parallel p-type quantum-well channels with base length up to 30 nm. An oscillation frequency, which depends on the base length, doping, and spatial period, as well as loads and voltage across the diode, ranges from $\leq$ 1 to 5 THz.**

**We propose an additional combined quantum GaAs–AlGaAs-heterostructure, which can be overgrown on a cleaved edge of a specially grown wafer. This structure is intended to obtain electron dispersion relations with NEM sections in the useful energy range of 0.1–0.25 eV.**

***Index Terms*—Ballistic transport, negative differential drift velocity, quantum-well device, semiconductor superlattice, terahertz oscillator.**

## I. Introduction

DESPITE every effort of numerous research groups, the so-called terahertz bandgap in the frequency band of high-efficiency compact solid-state sources has not been overcome, and these long-awaited sources require new efforts. Some people try to overcome this bandgap from the low-frequency direction using frequency multipliers. However, such a method also requires high-quality and high-power fundamental oscillators in subterahertz and near terahertz ranges. Among a great number of suggested fundamental oscillators, Gunn diodes (or transferred electron devices) still retain one of the leading positions (see [1] as a review). As is known, these diodes are based on globalization of negative-differential-drift-velocity (NDDV) instability in semiconductor diodes with an NDDV section in $v_D(E)$ [drift velocity electric field dependence; see Fig. 1(a)]. The conventional mechanism of NDDV (specifically, in GaAs and InP Gunn diodes) is the Ridley–Watkins–Hilsum (RWH) mechanism based on a multivalley electron spectrum. The idea of this mechanism is illustrated in Fig. 1(b) by means of the simplest two-valley model. In accordance with this mechanism, NDDV appears as a result of intervalley electron

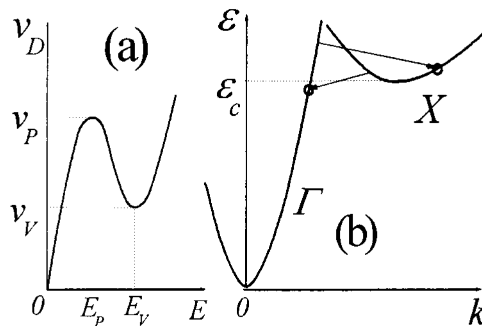


Fig. 1. (a) $v_D(E)$ dependence with an NDDV section. (b) Two-valley model of energy band spectrum illustrating the RWH mechanism.

scattering between the light-electron Γ-valley (effective mass $m$) and the heavy-electron $X$-valley (effective mass $M \gg m$). To create a high-frequency device, one has to provide a maximal rate of the intervalley $\Gamma X$-scattering and, especially, the reverse $X\Gamma$-scattering. A high rate of $\Gamma X$- and $X\Gamma$-scattering usually causes a high rate of any scattering for the energy region $\varepsilon \geq \varepsilon_C$ [see Fig. 1(b)]. Therefore, devices based on the RWH mechanism are structures with a substantially dissipative electron transport, which causes very large power losses. An increase in the frequency results in an increase in these power losses. We can observe this fact when moving from GaAs to InP, and further—from InP to GaN.

The RWH mechanism of NDDV, which is dominating in contemporary Gunn oscillators, is not the only one of its kind. Specifically, it is questionable that this mechanism can be realized in GaN devices. The authors of theoretical articles [2]–[5] derive $v_D(E)$ dependence with NDDV sections of the RWH origin for GaN. But the RWH mechanism in these calculations is foreseen from the start, since the electron band structure for GaN is presented in the form of an aggregation of several (up to three) independent valleys. This takes place for both a zinc blende (ZB) form and a wurtzite (W) form of GaN. Nonparabolicity of the electron spectrum in these valleys is taken into account with the help of the Kane model. In this model, an effective mass for high energies can become very large but cannot be negative. Intervalley scattering is the only mode of interaction between the valleys. In contrast to [2]–[5], in [6]–[8] the same transport problem is solved using full zone band structure full zone band structure (FZBS) calculations, resulting in the appearance of another mechanism of NDDV in both crystal forms of GaN. Such a result is conditioned by the existence of an inflection point boundary $\varepsilon_I(\vec{k})$, where an inverse differential effective mass of electrons moving along $\vec{k}$ becomes negative. Electrons with $\varepsilon > \varepsilon_I$ that move in

Manuscript received January 10, 2001; revised July 9, 2001. This work was supported by the National Science Foundation under Grant ECS-9813823 and the Air Force of Scientific Research under the MURI Program F4920-00-1-0328.

The authors are with the Department of Electrical and Computer Engineering, Wayne State University, Detroit, MI 48208 USA (e-mail: zinovi@ciao.eng.wayne.edu).

Publisher Item Identifier S 1077-260X(01)09935-X.

1077–260X/01$10.00 © 2001 IEEE

an electric field, which is antiparallel to $\vec{k}$, do not gain their velocity but lose it. As a rule, minimal values of $\varepsilon_I$ in ZB semiconductors occur in $\langle 111 \rangle$-directions (corresponding to electron motion from $\Gamma$-valley to $L$-valley across the separating saddle-point). An electron transfer across the inflection point boundary induces a new mechanism of NDDV called a negative-effective-mass (NEM) mechanism. The NEM mechanism can dominate over the RWH mechanism if the condition

$$\varepsilon_{I\ \min} < \varepsilon_X,\ \varepsilon_L \tag{1}$$

(where $\varepsilon_X$ and $\varepsilon_L$ are minimum energies in $X$- and $L$-valleys, respectively) is fulfilled with a certain reserve.

Note that the first suggestion to use negative effective masses in semiconductors for amplification and generation of electric oscillations was presented in the well-known letter of Kroemer [9] and in his extended article [10]. After many years, this suggestion led to the realization of the negative-effective-mass amplifier and generator (NEMAG) idea (see [11] as a review). Kroemer's NEMAG exploits NEMs, which occur in the parabolic spectrum region of heavy holes. In this case, the NEM is a result of warped forms of the isoenergetic surface of heavy holes. In contrast, the NEM mechanism of NDDV in GaN exploits a substantially nonparabolic spectrum region: $\varepsilon_{I\ \min}$ in GaN is equal to ~0.9 eV. An NDDV section for GaN is expected in electric fields ~100–200 kV/cm for the RWH mechanism (see [2]–[5] and [8]) and in some smaller fields for the NEM mechanism [6].

Electron dispersion relations obtained for different semiconductors in the FZBS approach convince anyone that (1) is satisfied not only for GaN but also for several other ZB-semiconductors; for example, for $In_{0.53}Ga_{0.47}$ As [12], [13], InAs [12], [14], and maybe for InP [14]. [Note that dispersion relations presented in graphic form in [12]–[14] do not always allow us to give the exact position of inflection points in the almost linear sections of dispersion curves $\varepsilon(k)$.] Of course, values of $\varepsilon_{I\ \min}$ in InAs, InGaAs, and InP are substantially lower than in GaN. For example, in InGaAs, we have $\varepsilon_{I\ \min} \sim 0.55$–0.6 eV versus ~0.9 eV in ZB GaN [6]. Unfortunately, we have no results related to NDDV oscillatory regimes (ORs) of the NEM-mechanism origin in the above-mentioned semiconductors. Such regimes would noticeably differ from analogous ORs of the RWH-mechanism origin, because they do not require any intervalley or intravalley scattering and exist due to electron drift in the electric field. This means that if we weaken any electron scattering for all the actual values of the energy, ORs of the NEM-mechanism origin are simpler to excite and reach a higher frequency. Therefore, a ballistic transport regime is the most preferable one. If all the other conditions are held constant, oscillation frequency must increase with an increase in an electric field.

From this point of view, results of theoretical articles [15], [16] are significant. The authors of [15] and [16] selected a certain model isotropic three-dimensional-hole dispersion relation (exploited before in [17]–[20]) in a $p^+pp^+$-structure and took into account all of the actual scattering mechanisms in the hydrodynamic approximation. (These mechanisms are described by typical parameters for GaAs.) A value of $\varepsilon_{I\ \min}$ is selected ≈0.1 eV. It is shown that the existence of an NEM section in $\varepsilon(k)$ almost definitely leads to the appearance of an NDDV section in $v_D(E)$. The stronger the increase in the effective mass in the NEM section, the more extended and expressive the NDDV section. These NDDV sections lead to stationary ORs, which are displayed for temperatures ≤220 K. A temperature fall as well as a decrease in the doping level activate the OR, since the weaker any kind of scattering, the more developed the OR. The dependence of an oscillation frequency on a voltage across a structure (or on a mean electric field) is of special interest: the frequency increases with the electric field (sometimes several times; for example, from 300 GHz to 1.2 THz in the diode with 0.5-$\mu$m-long p-base). Note that such behavior would be uncharacteristic for the RWN mechanism, but it is typical for the NEM mechanism, where a drift transfer from the light mass state to the heavy mass state takes place (that is, a drift deceleration instead of an intervalley scattering deceleration).

The limiting case of maximal speed for the NEM mechanism is a pure ballistic transport across a diode base. In this case, the intermediate concept of the drift velocity $v_D(E)$ (formed by joint action of different scattering mechanisms) becomes invalid, but an oscillation generation is quite realistic. It appears as a result of direct globalization of the NEM instability in a diode base [18]–[20]. But there are two basic reasons that can hinder such globalization.

First, the actual small lengths of ballistic transport taking place in real materials with an NEM section may not allow current carriers to excite the ballistic ORs. Second, we do not know of real NEM mechanisms with characteristic energies $\varepsilon_{I\ \min}$ in the range 0.1–0.25 eV. This range is preferable for obtaining high-efficiency oscillators, which exploit either the NEM mechanism of NDDV instability or utilize directly NEM instability in the ballistic limit. This range allows one to reach room-temperature ORs. But the NEM mechanisms known to us are either too low-energy (0.01–0.04 eV) or too high-energy (>0.6 eV).

In this paper, we consider just these two problems. In Section II, we consider ballistic regimes in a $p^+pp^+$-diode where the p-base is a system of modulation doping parallel quantum wells serving as current channels and separated from each other by isolating barriers. Since we consider a voltage range up to 0.1 V when base current carriers are able to emit optical phonons, we are especially interested in maximally short bases (up to 0.03 $\mu$m). In such bases, these events are almost improbable, and ballistic transport dominates. In Section III, we try to suggest a certain new method of dispersion relation design, which realizes NEM sections in the desirable range 0.1–0.25 eV. This suggestion anticipates sophisticated band structure engineering on the basis of modern nanostructures.

## II. Ultrashort Ballistic $p^+pp^+$-Diodes

### *A. Description*

A dispersion relation with an NEM section can be simply realized in a p-type quantum well (p-QW) with abrupt sidewalls, grown on the basis of diamond-like or ZB semiconductors. Symmetric square p-QWs are preferable. Dispersion relations for such QWs containing NEM sections for both the ground state and numerous excited states are repeatedly predicted [21]–[24]. The predicted dispersion relations are qualitatively

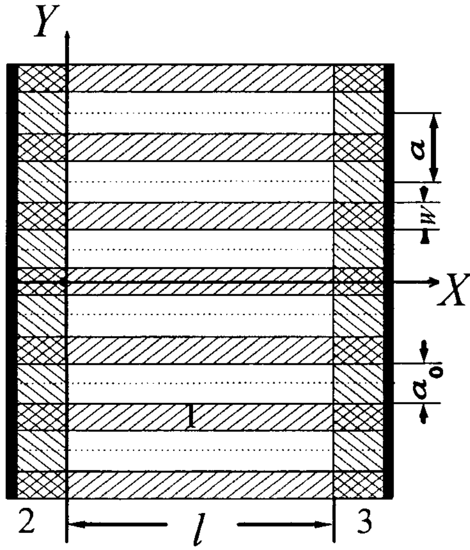


Fig. 2. $p^+pp^+$-diode in the form of a system of parallel p-QW channels separated by barriers with modulation doping sheets (dashed lines). 1: p-base, 2: $p^+$-source (emitter), and 3: $p^+$-drain (collector).

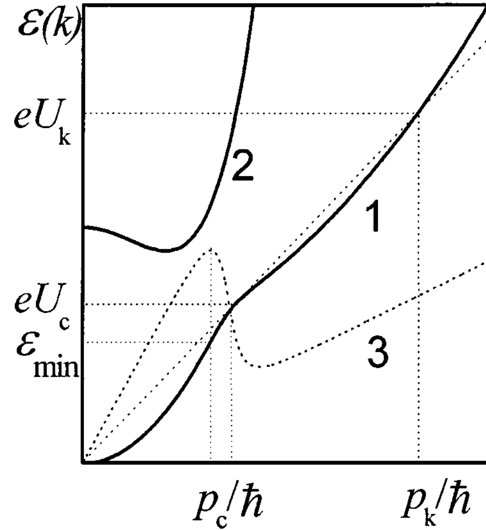


Fig. 3. Dispersion relation $\varepsilon(k)$ for 8-nm-thick GaAs–AlAs p-QW. 1: The ground quantization subband; 2: the first excited quantization subband; and 3: the velocity $v(k) = \hbar^{-1}\partial\varepsilon/\partial k$ in the ground subband.

confirmed in resonance magnetotunneling of holes through p-type double barrier resonant-tunneling structures [25]–[27]. Although transport properties of p-QWs are traditionally less effective than those of n-QWs, it is well known that high-record values of hole mobility (up to $1.2 \times 10^6$ cm$^2$/Vs in [28]) were repeatedly reported for modulation doped p-GaAs–AlGaAs QWs grown on specially oriented $\langle 311 \rangle$ A GaAs substrates. It is true that such high values of hole mobility are reached either in quasi-triangle QWs [28]–[31] or in very thick square QWs [29], [34], where the hole gas is of the same structure as in the triangle wells. [Note that very high hole mobilities are also measured in double hole gas systems [34], [35], in which p-GaAs QWs are separated by AlGaAs barriers. In [35], mobilities in each of 15-nm-thick wells are equal to $\sim 10^6$ cm$^2$/Vs (T $=$ 30 mK) at the barrier thickness 2.0–3.5 nm.] But values $\sim 5 \times 10^4$–$10^5$cm$^2$/Vs that are obtained for 6–8 nm thick square p-QWs [32], [33] are also satisfactory for considered diode structures. Unfortunately, even in these thin wells, values of $\varepsilon_{I\ \min}$ ($\sim$0.02–0.04 eV) are too small for the oscillators to be effective outside of the cryogenic temperature region. An increase in $\varepsilon_{I\ \min}$ requires a further decrease in QW thickness. In turn, this leads to a further decrease in ballistic lengths because additional sidewall roughness scattering occurs. We also do not have a sufficient reserve of barrier height for p-GaAs QW sidewalls (in the GaAs–AlAs system). Decreasing thickness up to $\leq$4–5 nm does not lead to any increase in $\varepsilon_{I\ \min}$.

Although ORs can be obtained in solitary p-QWs, the best results (the shortest base lengths and the highest oscillation frequencies) occur for a system of parallel QWs separated by very thin barriers. By using the system of parallel QW channels (Fig. 2), we minimize parasitic capacity related to one channel. This capacity per channel is smaller if channels are placed closer to each other. The effect of parasitic side capacities is lessened if a number of united QW channels in the multichannel device are greater. In fact, the limiting case $a_0 \to 0$ would be best ($a_0$ is a barrier thickness), but it is impossible to obtain because we must protect a two-dimensional (2-D) hole gas in the QWs. A tunnel transparence of barriers leads to a decrease in $\varepsilon_{I\ \min}$ and to the smearing of NEM sections. We also need to avoid or to diminish scattering of holes by ionized acceptors. Therefore, we need modulation doping and sufficiently thick barriers to provide this doping.

Further results are obtained only for a periodic system of QW channels. Concentrations of acceptors and holes (cm$^{-2}$), current density (A/cm$^2$), and parameters of external and internal electric circuit (resistance, $\Omega$ cm; capacitance, pF/cm; inductance, pH cm) are indicated per one channel and per unit of width. All calculations are performed for 8-nm-thick p-type square GaAs–AlAs QW. In this well, quantized states are calculated using the simplest two-band isotropic approximation ($4 \times 4$ Hamiltonian). It is sufficient to calculate the required ground quantization state (and may also be sufficient for the first excited state; see Fig. 3). The following Luttinger parameters have been used: $\gamma_1 = 6.9$, $\gamma_2 = \gamma_3 = 2.5$ for GaAs and $\gamma_1 = 4.0$, and $\gamma_2 = \gamma_3 = 1.3$ for AlAs. The height of sidewalls (discontinuity) is taken to be 0.5 eV. The QW thickness is selected so that almost the entire so-called classic generation interval $(eU_C, eU_K)$ is placed below the energy of an optical phonon in GaAs (0.036 eV). In the future, we will see that the generation occurs far out of the limits of the generation interval mentioned above, at $U > U_K$ (see also [36]).

ORs are investigated in detail for two values of barrier thickness: $a_0 = 32$ and 16 nm (so spatial periods $a = a_0 + w$ are equal to 40 and 24 nm, respectively). Since we assume only ballistic hole transport in the p-QW channels, holes cannot escape from these channels even if their energy exceeds the barrier height (this is excluded in the presented results). Therefore, holes stay only in the QWs.

### *B. Base Length Dependence. Classic and High-Voltage Regimes*

In unloaded diodes with the given voltage drop $U$ between $p^+$-contacts, ORs appear beginning with a certain minimal

(threshold) base length $l_m$, which depends on doping $N_A$, space period $a$, and loads in an external circuit. If such loads are absent (short-circuit regime), $l_m = l_m(0) \cong$ 65–70 nm for $N_A = 10^{11}$ cm$^{-2}$ and $a = 40$ nm and $l_m(0) \cong$ 40–45 nm for the same value of $N_A$ and $a = 24$ nm. An increase in $N_A$ up to $2 \times 10^{11}$ cm$^{-2}$ for $a = 24$ nm leads to a decrease in $l_m(0)$: $l_m(0) \cong$ 30–35 nm. External inductive loads in a certain range of values substantially activate an OR [37]. Therefore, minimal base lengths $l_m(L)$ of OR existence can be noticeably decreased in comparison with $l_m(0)$ (see below). These minimal base lengths are smaller than hole mean free paths in p-QWs with the above-presented parameters and mobility $\geq$50 000 cm$^2$/Vs. But they are greater than the mean free paths of emitted light holes in bulk GaAs that were experimentally measured in [38]. Rapid transfer of emitted light holes into heavy hole states (by means of numerous scattering mechanisms, including an optical phonon emission) explains the small size of the paths measured in [38]. In our specific case of quantized 2-D holes (not bulk holes), such transfer is impossible because the ground quantized hole subband is itself genetically a heavy hole subband. Small effective mass values in this subband (for small values of 2-D momentum) appear as a result of spin-orbital interaction in quantum-well sidewalls. In this case, emission of optical phonons must be substantially suppressed in comparison with the bulk case, since as a result of this emission, holes transfer into states with a minimal effective mass. The most dangerous scattering mechanisms for this case are an elastic roughness scattering and an elastic scattering on ionized acceptors (placed in sheets in the middle of extremely thin barriers). As a result of such scattering, most NEM holes survive as NEM holes. Of course, this scattering can affect some parameters of ORs (can narrow a frequency band). But (in accordance with results of [15] and [16]) ORs in such diodes are quite probable.

In the shortest base diodes, ORs occur only in the voltage interval $(U_C, U_K)$. These are classic ORs. Along with them, there exist the so-called high-voltage ORs, which occur when $U > U_K$. The classic OR is a result of globalization of convective NEM instability in an NEM quasi-neutral region of the base, where a negative acceptor charge is accurately compensated by a positive NEM-hole charge. Such an NEM quasi-neutral region is possible only inside the interval $(U_C, U_K)$. An appearing OR disrupts the quasi-neutrality by forming charged enhanced and depleted layers and causing their drift across this region. The time-depending voltage $U_{SC}(t)$ drops on drifting charged layers. Therefore, the rest of the voltage $U - U_{SC}(t)$ dropping on a source-adjacent space-charge region also depends on time. It leads to oscillations of emitted current, which is controlled by this voltage.

The high-voltage OR appears at $U > U_K$ when the NEM quasi-neutral region disappears. All of the NEM holes are collected in a narrow accumulation layer inside the above-mentioned source-adjacent space-charge region. Only heavy and light positive mass holes exist in the quasi-neutral region. They form two different streams with different velocities and energies. The first stream consists of hot ballistic holes, which come from the p$^+$-source (emitter) and become heavy after passing the accumulation layer. The second stream consists of light holes, which are in equilibrium with the p$^+$-drain (collector) hole reservoir. Instability leading to the high-voltage OR is initially displayed in the form of a position and charge instability of the accumulation layer inside the space-charge region. Oscillations of the accumulation layer induce spatial charge waves, which spread to the quasi-neutral region with the two above-mentioned hole streams. The longer the base, the greater the oscillation amplitude and the more extended the high-voltage interval of the oscillations. As a result, a hypothesis emerges that a two-stream instability [39] plays a role in the formation and development of the high-voltage OR. This instability just occurs precisely in extended quasi-neutral plasmas with current carriers of two types with different drift velocities. If this is true, the source-adjacent space-charge region with the unstable accumulation layer serves as an initial generator, and the quasi-neutral region serves as an amplifier. Note that an oscillation frequency in long base diodes for the high-voltage regime can be noticeably higher than in the much shorter base diodes, where only the classic regime can be possible.

### C. *Inductive Load Dependence*

Voltage limits and current oscillation amplitudes of both ORs can be substantially developed by means of an inductive load [37]. An increase in a loading inductance $L$ first increases the amplitude of current oscillations. The amplitude approaches a maximal value at a certain value $L = L_{\text{opt}}$. A further increase in $L$ gradually suppresses the OR that disappears at some $L = L_M$. In shorter base diodes, using a loading inductance can activate (beginning from a certain value $L = L_m$) a certain OR that would not exist at $L < L_m$. An inductive load influences not only current oscillation amplitude but also oscillation frequency: as a rule, an increase in $L$ leads to lowering of frequency. The effect of a loading inductance differs for classic and high-voltage regimes. On the whole, the classic regime is controlled by visibly greater values of $L$ than the high-voltage one. Therefore, in diodes where both regimes can be activated, an increase in $L$ initially activates the high-voltage regime and brings it to the highest level of development. A further increase in $L$ leads to the deactivation of the high-voltage OR (up to complete suppression) but continues to develop the classic regime. Optimal ($L_{\text{opt}}$) and maximal ($L_M$) values for these two regimes can drastically differ from each other. This different reaction to inductive loads also gives evidence of participation of an additional instability mechanism in forming the high-voltage OR.

Inductive load influences not only current oscillation amplitudes but also oscillation frequencies. The dependence of oscillation frequency on the base length $l$ in the diode with $a =$ 24 nm for several values of $L$ is depicted in Fig. 4. This dependence is calculated for a fixed value of the voltage, 25 mV (for the classic regime). We can see that the oscillation frequency in the classic regime monotonically decreases with the base length. It also noticeably (but ambiguously) depends on $L$ for the shorter base diode ($l \leq 0.08$ $\mu$m). In Fig. 5, an oscillation frequency in the same diodes is depicted depending on an inductance $L$ for base-lengths of 0.04, 0.045, 0.05, 0.055, and 0.06 $\mu$m. The 0.04- and 0.045-$\mu$m-long base diodes are able

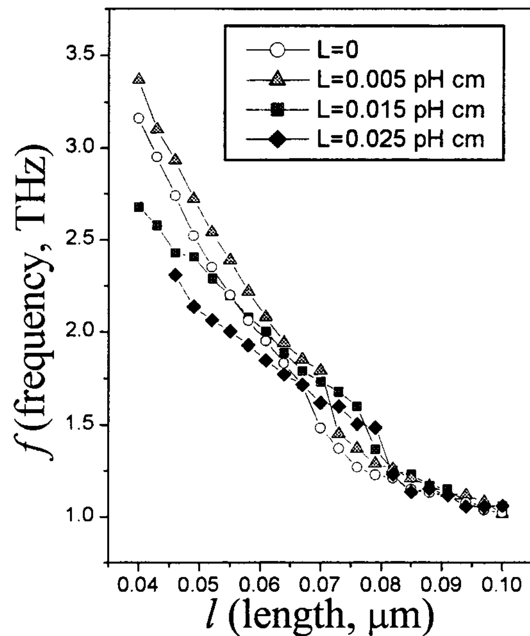


Fig. 4. Dependence of oscillation frequency $f$ on the base length $l$ for $U = 25$ mV and $L = 0, 0.005, 0.010, 0.015$, and $0.025$ pH cm.

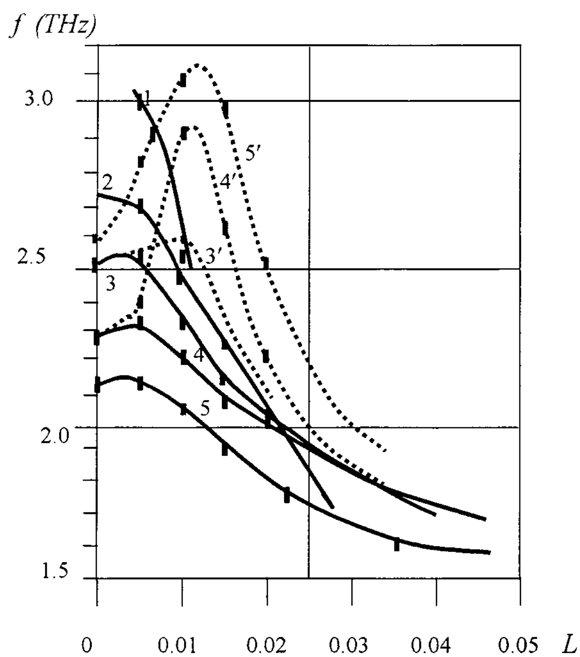


Fig. 5. Dependence (sketch) of oscillation frequency $f$ on inductance $L$ for several base lengths $l : l = 0.04$ $\mu$m (1), $0.045$ $\mu$m (2), $0.05$ $\mu$m (3 and 3′), $0.055 \mu$m (4 and 4′), and $0.06 \mu$m (5 and 5′). Solid curves are for classic ORs. Dashed curves are depicted for high-frequency limits of high-voltage ORs.

to oscillate only in the classic regime (and the 0.04-$\mu$m-long base diode can oscillate only with an inductive load in the small range 0.005–0.01 pH cm). Oscillation frequency bands of these two diodes are very narrow and are represented by the mean frequency values in Fig. 5. The 0.055- and 0.06-$\mu$m-long base diodes oscillate in both classic and high-voltage regimes. Some high-voltage regime signs are also presented in the OR of the 0.05-$\mu$m intermediate long base diode. We see in Fig. 5 both

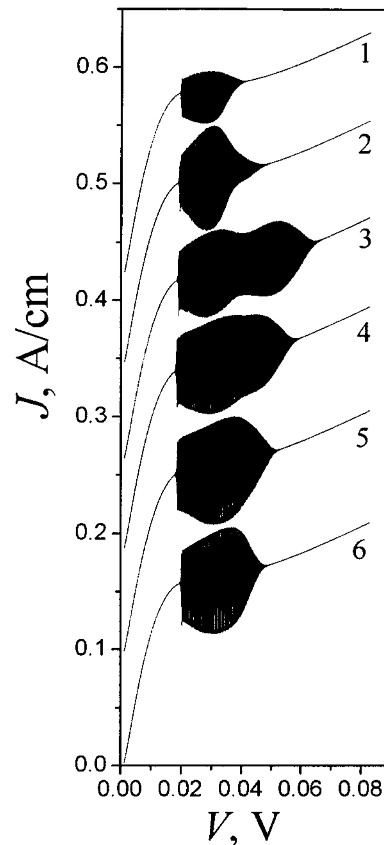


Fig. 6. Oscillatory portraits for 0.055-$\mu$m-long base diode ($a = 24$ nm) at $L = 0$ (1), $0.005$ (2), $0.010$ (3), $0.015$ (4), $0.020$ (5), and $0.025$ (6) pH cm. Curves are approximately 0.1 A/cm shifted relating to each other for convenience.

the lower frequency classic-region dependence on $L$ and the higher frequency maximal high-voltage-region dependence on $L$. The latter is substantially nonmonotonic (of evident resonance character), and the frequency increases extraordinarily with an increase in the base length. The oscillatory portraits of ORs, "measured" for an adiabatically slow increase in the voltage across the 0.055-$\mu$m-long base diode, are presented in Fig. 6. The Fourier portraits of these oscillations are shown in Fig. 7. We can see that there are very large second harmonics of oscillations ($f \cong 4.7$ THz) at $L = 0$ and especially 0.005 pH cm. (For $l = 0.06$ $\mu$m, this second harmonic exceeds the fundamental frequency amplitude.) The high-voltage regime is maximally displayed at $L = 0.01$ pH cm: the second harmonic is relatively suppressed, but the fundamental frequency band extends in an unusual way. There may be a gradual voltage tuning of the frequency in the range from 2 to 3 THz. (This range is even wider for the 0.06-$\mu$m-long base diode.)

Further extension of the diode base length leads to a further development of the high-voltage OR. In the background of the power high-voltage regime, the classic regime is lost and becomes unstable. For example, oscillation frequency in the classic regime is $\sim$1.2 THz at $L = 0$ and decreases up to $\leq$1 THz at $L = 0.3$ pH cm in the 0.08-$\mu$m-long base diode. In the high-voltage regime, oscillations with much greater amplitude are tuned by the voltage in the range of 2.2–2.8 THz at $L = 0.017$ pH cm in the same diode.

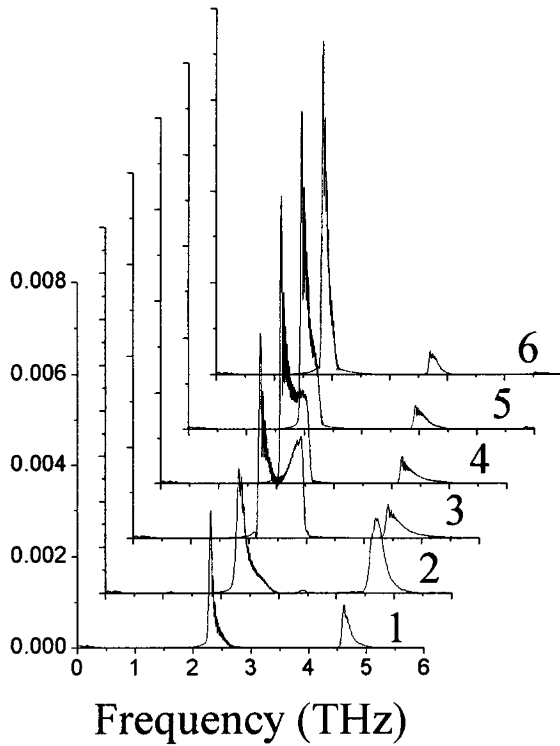


Fig. 7. Fourier portraits of the oscillatory regimes presented in Fig. 6.

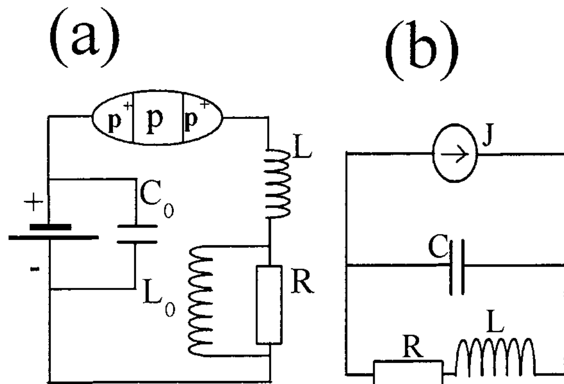


Fig. 8. (a) $p^+pp^+$-diode in the electric circuit. (b) Equivalent circuit for calculation of high-frequency power and efficiency.

### D. Resistive Load Dependence and Efficiency

We can also see different behavior of two oscillatory regimes for active loads in the external circuit. Naturally, active loads, which are needed to obtain a useful high-frequency power and reach a maximal efficiency, lead to decreasing amplitudes of current oscillations. We study the mutual influence of inductive and active loads on the basis of the electric circuit shown in Fig. 8(a). This circuit includes the diode, inductor $L$, active resistor $R$, dc voltage source $U_0$, and two additional elements: a very large inductor $L_0$, which shunts resistor $R$ on a direct current (but $2\pi f L_0 \gg R$ where $f$ is a frequency), and capacitor $C_0$, which shunts the voltage source on a high-frequency current. This circuit provides dc voltage $U_0$ across the diode and liberates a power $\overline{J}U_0$, where $\overline{J}$ is a mean value of current (that is, a dc component) in the diode. Besides a dc component, there exists an alternating (high-frequency) component $J(t)$ in each cross-section $x$ of the diode. It can be represented as a sum of convective hole current in the channels $J_C(x, t)$ and a capacitive current

$$J(t) = J_C(x, t) + \frac{\partial}{\partial t}\int_{-a/2}^{a/2} D_x(x, y, t)\, dy \qquad (2)$$

where $\vec{D}$ is an electrostatic induction. [Remember that a current is really a current density per unit of width in the third (Z) direction and per channel.] As a result of integration of both sides of (2) on $x$ from zero to $l$, we obtain

$$J(t) = \tilde{J}_C(t) + C\frac{\partial}{\partial t}U \qquad (3)$$

where $\tilde{J}_C(t) = (1/l)\int_0^l J_C(x, t)\, dx$ is a mean convective current in the diode base and $C = a\kappa_D/l$ is a capacity of one spatial period of our periodic device. Note that $\kappa_D$ is some effective dielectric constant of our inhomogeneous (layered) system. Equation (3) shows that our problem is reduced to the simulation of a circuit shown in Fig. 8(b), where alternating current source $\tilde{J}_C$ supplies connected in parallel capacitor $C$ in one branch and resistor $R$ in series with inductor $L$ in another branch. In the case of harmonic current $\tilde{J}_C(t) = \tilde{J}_{CM}\cos 2\pi f t$, efficiency of a diode oscillator can be described by the formula

$$\eta = \frac{\tilde{J}_{CM}^2 R}{2\overline{J}U_0\{[1-(2\pi f)^2 LC]^2 + (2\pi f CR)^2\}}. \qquad (4)$$

In (4), $\overline{J}$depends in practice only on $U_0$, but $\tilde{J}_{CM}^2$ and frequency $f$ are functions of all the parameters of the external circuit, $L$, $R$, and $U_0$. These functions, calculated numerically, show that not only inductance $L$ but also resistance $R$ influence $\tilde{J}_{CM}^2$, $f$, and finally $\eta$ much more noticeably in the high-voltage regime than in the classic one.

We calculate a maximal efficiency $\eta$ for the 0.05-$\mu$m-long base diode in the classic regime ($U = 25$ mV). It is reached at $L = L_0 = 0.012$ pH cm and $R = R_0 = 0.077$ $\Omega$cm and equal to $\eta_M = 0.75\%$. An oscillation power is $3 \times 10^{-5}$ W/cm. If $L = 0$, we obtain $R = R_0 = 0.11$ $\Omega$cm, and efficiency is two times less.

### E. Spatial Period and Doping

Turning from the shorter period $a = 25$ nm to the longer period $a = 40$ nm shifts threshold (minimal) base lengths $l_m$ to the longer base side: for example, $l_m(0)$ becomes ~0.07 $\mu$m instead of ~0.045 $\mu$m obtained above. An increase in $a$ induces a decrease in oscillation frequencies. This can be explained by an increase in capacity $C$ per one (extended) spatial period and one current channel.

An increase in doping per channel leads to a decrease in threshold base lengths $l_m$: switching from $10^{11}$ cm$^{-2}$ to $2 \times 10^{11}$ cm$^{-2}$ induces a decrease in $l_m(L)$ up to $\leq$30 nm. Oscillatory regimes also depend on $p^+$-region doping (see [36]).

## III. Dispersion Relations with the NEM Sections

As indicated in the Introduction, the wide use of NEM mechanisms of the NDDV and NEM ballistic generators is impeded by a lack of proper natural NEM-contained dispersion relations

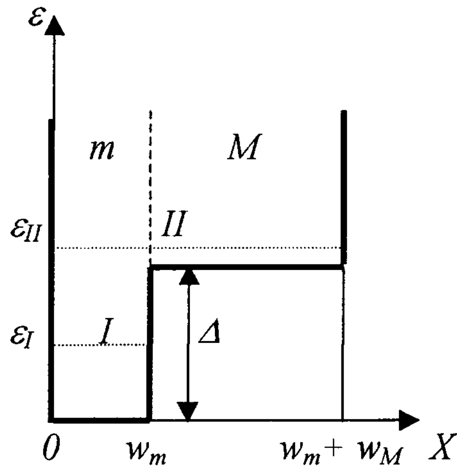


Fig. 9. Combined heterostructural QW consisted of two layers with different longitudinal (in-plane) electron effective masses ($m$ and $M$).

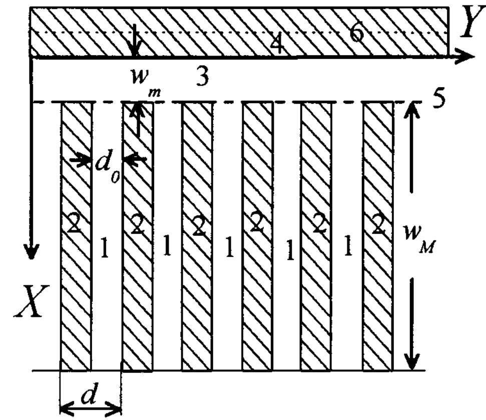


Fig. 10. Schematic heterostructure (with NEM dispersion relation) grown on a cleaved edge. 1: GaAs QW layers grown at the first growth; 2: AlGaAs barrier layers grown at the first growth; 3: GaAs QW layer (the dipper layer) grown at the second growth; 4: AlGaAs barrier grown at the second growth; 5: plane of the cleaved edge; and 6: modulation donor doping sheet.

with the optimal range of $\varepsilon_{I\,\min}$ (≅0.1–0.25 eV). Therefore, a suggestion that such mechanisms are feasible by means of quantum engineering is productive. One of the evident methods to obtain the desirable result is an electron quantization in a combined heterostructure quantum well shown in Fig. 9 and consisting of two layers with different dynamic parameters. These layers must be specially selected: one of them (left) is energetically deeper and another is energetically shallower. They should be chosen so that the ground quantization state (sublevel I in Fig. 9) would be localized at $\vec{k} = 0$ almost completely in the deeper one and the first excited state (sublevel II) would be expanded in both layers (and a substantial part of the electron density would be in the shallower one). A longitudinal effective mass $m$ in the plane of the deeper layer should be much smaller than the analogous effective mass $M$ in the shallower layer: $m \ll M$. Such a difference in the effective mass leads to unavoidable intersection of terms II and I with increasing $k$ and to their anticrossing. As a result of such anticrossing, the combined ground state contains the expected NEM section. The above-described method of NEM-section formation can be called a quantum real-space transfer (QRST). Through the gaining of kinetic energy, the electron wave function shifts from the small effective mass deeper layer to the shallower layer II with its very large longitudinal effective mass of electrons. The QRST (contrasting to a conventional or classic RST [40], [41]) is a collisionless and nondissipative process. It leads to the NDDV only through additional secondary dissipative phenomena. Unfortunately, a list of materials, which are appropriate for the deeper and narrower layers and simultaneously for a high-quality epitaxial growth of multilayer (or at least two-layer) heterostructures, is very poor. For example, we cannot obtain a necessary big difference between masses $m$ and $M$ either in the traditional $\Gamma\Gamma$–GaAs–$Al_xGa_{1-x}As$ structure ($x < 0.45$) or in the InP–InGaAs–InAlAs structure. Such a difference is sufficiently great in the $\Gamma X$–GaAs–$AlxGa_{1-x}As$ structure ($x > 0.45$), but in this case, a small factor occurs for the direct $\Gamma X$ transition (without any scattering) in an abrupt $\Gamma X$ border.

Further, we should focus upon one more version of $\Gamma\Gamma$–GaAs–$Al_xGa_{1-x}As$ structure, which can lead to the required result. Since 1990, a number of experiments were devoted to researching different 2-D electron and hole structures grown on cleaved edges of a GaAs wafers, which can also contain some heterostructures [42]–[47]. This technology allows one to grow a heterostructure schematically depicted in Fig. 10. The GaAs quantum-well 3 overgrown directly on the cleaved edge and covered by the modulation-doped AlGaAs barrier 4 (grown on the top) plays the role of the dipper layer I (from Fig. 9). The superlattice grown as a result of the first growth (on a GaAs wafer) and formed by the alternating of GaAs QWs 1 and AlGaAs barriers 2 plays the role of the shallower layer. Naturally, a dispersion relation of the superlattice is very anisotropic. It can be characterized by the same effective mass $m$ as in QW 3 along the $X$ axis and has a miniband character along the $Y$ axis. We consider the case of narrow minibands, so an effective mass along the axis Y can be assumed to be very large: $M \gg m$. If the superlattice period $d \ll w_m$ (Fig. 10), the superlattice can be presented as an anisotropic homogeneous medium. An electron dispersion relation in the structure shown in Fig. 10 (with a finite size $w_M$) can be calculated as an electron dispersion relation in the combined QW from Fig. 9 with an isotropic mass $m$ in the deeper layer and with an anisotropic mass in the shallower layer: $m_{xx} = m$ and $m_{yy} = M \gg m$. We assume $M = \infty$ for simplification. As a result of such a procedure, we intentionally lose all the quantum wire and miniband effects, which are not relevant to our problem concerning the NEM spectrum. The boundary conditions

$$\Psi(0, y) = \Psi(w_m + w_M, y) = 0$$
$$\Psi(w_m - 0, y) = \Psi(w_m + 0, y)$$
$$\left.\frac{\partial\Psi}{\partial x}\right|_{w_m - 0} = \left.\frac{\partial\Psi}{\partial x}\right|_{w_m + 0}$$

lead to the dispersion equation

$$\frac{\tan\sqrt{\varphi - \kappa^2}}{\sqrt{\varphi - \kappa^2}} = -\frac{\tan\delta\sqrt{\varphi - \varphi_0}}{\sqrt{\varphi - \varphi_0}} \tag{5}$$

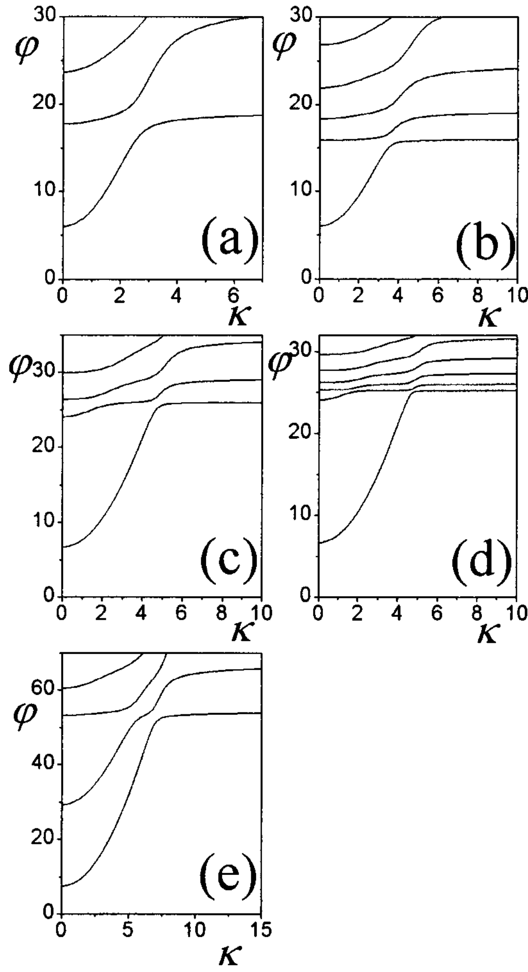


Fig. 11. Dispersion relations $\varphi = \varphi(\kappa)$ followed from (5). (a) $\varphi_0 = 15$, $\delta = 1.5$; (b) $\varphi_0 = 15, \delta = 3.0$; (c) $\varphi_0 = 25, \delta = 3.0$; (d) $\varphi_0 = 25, \delta = 6.0$; and (e) $\varphi_0 = 50, \delta = 1.5$.

where $\Psi(x, y)$ is a wave function

$$\varphi = \frac{2m\varepsilon w_m^2}{\hbar^2}, \quad \kappa = w_m k, \quad \varphi_0 = \frac{2m\Delta w_m^2}{\hbar^2}$$

where $\delta = w_M/w_m$ and $\varepsilon = \varepsilon(k)$ is the desired dispersion relation. The dependence $\varphi = \varphi(\kappa)$ determined by (5) is presented in Fig. 11 for four sets of parameters $\varphi_0$ and $\delta$. Among these parameters, a value of discontinuity $\Delta$ (see Fig. 9) requires a certain clarification. It is some schematic value, which is determined by the energy of the lowest miniband in the above-considered superlattice (Fig. 10). For tunnel-nontransparent barriers 2, we obtain

$$\Delta \cong \frac{\pi^2\hbar^2}{2md_0^2}. \tag{6}$$

In accordance with the assumed concept, thickness $d_0$ must be much smaller than thickness $w_m$. Then $\varphi_0/\varphi(0) \approx (w_m/d_0)^2 \gg 1$. In our results in Fig. 11, we obtain $\varphi_0/\varphi(0) \approx 2.5, 3.5$, and 7.0. The third value takes place with an additional intermediate subband of quantization [Fig. 11(e)], and it is undesirable. This means that we can provide in practice only a range $2d_0 \geq w_m > d_0$, and weak

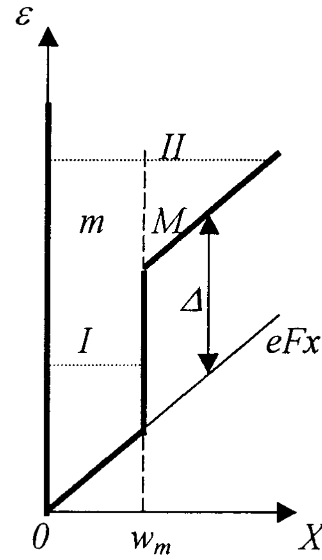


Fig. 12. Heterostructural QW in the constant transverse electric field.

quantum wire effects are unavoidable. They lead to a moderate increase in the longitudinal effective mass in the basic QW 3.

In fact, it is very difficult to form technologically a finite size $w_M$. However, we can obtain a satisfactory similarity of the necessary two-layer combined quantum well if we take into account the above-assumed modulation donor doping of the AlGaAs barrier 4 together with the additionally assumed acceptor doping of the superlattice in Fig. 10. In such a combination, there appears a quasi-triangle potential profile formed in the depletion layer. This profile restricts the spreading of the electron wave functions along the $X$ axis (Fig. 12). The dispersion relations of electrons in this structure, calculated in the approximation of a constant transverse electric field, are obtained from the dispersion equation (7), as shown at the top of the next page, where $\mathrm{Ai}\,(x)$ and $\mathrm{Bi}\,(x)$ are Airy functions of $x$, $\mathrm{Ai}'(x)$ and $\mathrm{Bi}'(x)$ are their derivatives (see [46])

$$\varsigma = \frac{2meFw_m^3}{\hbar^2}$$

and $F$ is an electric field. Several calculated dispersion relations are depicted in Fig. 13 for different satisfactory sets of $\varphi_0$ and $\varsigma$. Simultaneous increases in both $\varphi_0$ and $\varsigma$ lead to the appearance of the second sublevel in QW 3.

Naturally, the presented evaluations of spectra $\varepsilon(k)$ are very approximate. In reality, we need to reject the effective medium approximation for the superlattice and to consider a detailed heterostructural potential in it. Such an approach would allow us to take into account quantum wire effects. We need also to calculate a realistic electric potential dependent on screening the electric field by free electrons (that is, to solve a self-consistent Poisson–Schrödinger problem). As a result, we could calculate accurate values of both the modulation donor doping in barrier 4 and the acceptor doping of the superlattice. Note that the acceptor atoms can be placed only inside the barrier layers 2 during the growth of the superlattice. It attenuates the scattering of electrons by the ionized acceptors (whose mean concentration in the superlattice is $\geq 10^{17}$ cm$^{-2}$ if an electron concentration in the considered structure exceeds $10^{11}$ cm$^{-2}$).

$$\frac{\mathrm{Bi}(\varsigma^{-2/3}(\kappa^2-\varphi))\mathrm{Ai}'(\varsigma^{-2/3}(\kappa^2-\varphi)+\varsigma^{1/3})-\mathrm{Ai}(\varsigma^{-2/3}(\kappa^2-\varphi))\mathrm{Bi}'(\varsigma^{-2/3}(\kappa^2-\varphi)+\varsigma^{1/3})}{\mathrm{Bi}(\varsigma^{-2/3}(\kappa^2-\varphi))\mathrm{Ai}(\varsigma^{-2/3}(\kappa^2-\varphi)+\varsigma^{1/3})-\mathrm{Ai}(\varsigma^{-2/3}(\kappa^2-\varphi))\mathrm{Bi}(\varsigma^{-2/3}(\kappa^2-\varphi)+\varsigma^{1/3})} = \frac{\mathrm{Ai}'(\varsigma^{-2/3}(\varphi_0-\varphi)+\varsigma^{1/3})}{\mathrm{Ai}(\varsigma^{-2/3}(\varphi_0-\varphi)+\varsigma^{1/3})} \quad (7)$$

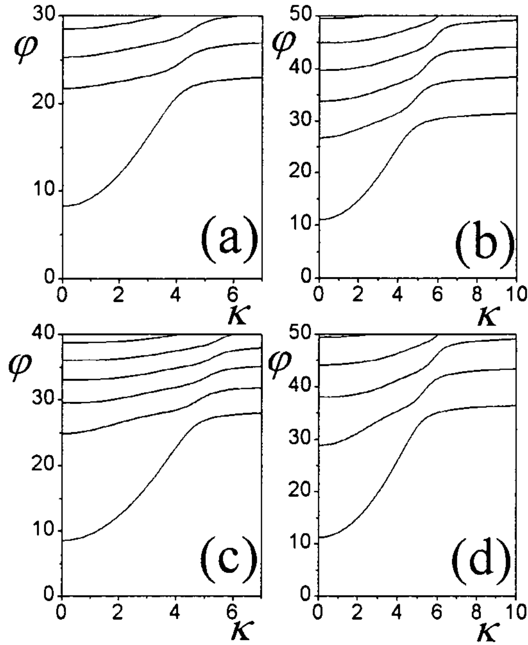


Fig. 13. Dispersion relations $\varphi = \varphi(\kappa)$ followed from (7). (a) $\varphi_0 = 15$, $\varsigma = 1.5$; (b) $\varphi_0 = 15, \varsigma = 2.0$; (c) $\varphi_0 = 20, \varsigma = 1.5$; and (d) $\varphi_0 = 20$, $\varsigma = 2.0$.

The main disadvantage of the presented cleaved edge design is the practical impossibility to grow a system of close parallel channels (as in Fig. 2). However, note that the shift of $\varepsilon_{I\ \min}$ from 0.015 eV to, for example, 0.15 eV enhances the oscillation power a dozen times.

## IV. Concluding Remarks

There are two actual mechanisms of NDDV and subterahertz and terahertz range generation on the basis of NDDV: the RWH mechanism and the NEM mechanism. The second of them is suitable for direct excitation of oscillations aside from the intermediate NDDV stage. These mechanisms have no evident advantages for implementation of Gunn generators on the basis of GaN and analogous materials. But in general, these are noticeably different mechanisms. The RWH mechanism contains an intervalley scattering inside: the greater the rate of this scattering, the higher the speed of devices based on this mechanism. To increase the speed of RWH-mechanism-based devices, we must increase the power dissipated in them. The NEM mechanism is based on a drift transfer to a falling branch of a $v_D(E)$-dependence. Therefore, the lower the scattering rates, the higher the device speed. A maximal speed can be reached without any scattering, meaning use of ballistic electron transport. An example of such transport for ultrashort $p^+pp^+$-diodes with p-QW bases is considered in detail in Section II. Ballistic transport allows electrons to reach especially high transport velocities at much (~3 times) lower electric fields (that is, at smaller voltages across the diode than for dissipative transport NDDV mechanisms). Electron energies, which form the NDDV section, can be decreased from 0.5–0.9 eV in the contemporary Gunn diodes to 0.1–0.25 eV in the desirable room-temperature NEM diodes.

NEM sections in dispersion relations of natural $A_3B_5$ and $A_2B_6$ semiconductors with ZB and wurtzite crystal lattices are displayed at energies that are too high (> 0.5 eV) to obtain high-mobility low-dissipative electron transport. In p-QWs of acceptable thickness (for high-mobility transport), one gets NEM sections that are too low-energy and allow only low-temperature small-power terahertz generation. This means that growing high-mobility structures with NEM sections in the intermediate energy region is a very vital problem. Such structures should 1) protect sufficiently large ballistic lengths, 2) shift generation in the room-temperature direction, and 3) significantly increase oscillation power per one channel. A possible example of such a structure, using QRST in a two-layer QW, one of which is a superlattice finite-size layer, is considered in Section III.

## Acknowledgment

The authors would like to thank Prof. G. I. Haddad and Dr. H. Eisele from the University of Michigan for valuable discussion and support. They also thank Dr. N. Z. Vagidov and Dr. D. Romanov from Wayne State University and O. Melnikova from the University of Michigan for friendly help.

## References

[1] H. Eisele and G. I. Haddad, “Two-terminal millimeter-wave sources,” *IEEE Trans. Microwave Theory Tech.*, vol. 46, pp. 739–746, June 1998.
[2] B. Gelmont, K. Kim, and M. Shur, “Monte Carlo simulation of electron transport in gallium nitride,” *J. Appl. Phys.*, vol. 74, pp. 1818–1821, Aug. 1993.
[3] N. S. Mansour, K. W. Kim, and M. A. Littlejohn, “Theoretical study of electron transport in gallium nitride,” *J. Appl. Phys.*, vol. 77, pp. 2834–2836, Mar. 1995.
[4] U. V. Bhapkar and M. S. Shur, “Monte Carlo calculation of velocity-field characteristics of wurtzite Ga N,” *J. Appl. Phys.*, vol. 82, pp. 1649–1655, July 1997.
[5] B. E. Foutz, S. K. O'Leary, M. S. Shur, and L. F. Eastman, “Transient electron transport in wurtzite Ga N, In N, and Al N,” *J. Appl. Phys.*, vol. 85, pp. 7727–7734, June 1999.
[6] S. Krishnamurthy, M. van Schlifgaarde, A. Sher, and A.-B. Chen, “Bandstructure effect on high-field transport in Ga N and Ga Al N,” *Appl. Phys. Lett.*, vol. 71, pp. 1999–2001, Oct. 1997.
[7] C. Bulutay, B. K. Ridley, and N. A. Zakhleniuk, “Comparative analysis of zinc-blende and wurtzite Ga N for full-band polar phonon scattering and negative differential conductivity,” *Appl. Phys. Lett.*, vol. 77, pp. 2707–2709, Oct. 1997.
[8] J. Kolnik, I. H. Oguzman, K. F. Brennan, R. Wang, P. P. Ruden, and Y. Wang, “Electronic transport studies of bulk zinc-blende and wurtzite phases of Ga N based on an ensemble Monte Carlo calculation including a full zone band structure,” *J. Appl. Phys.*, vol. 78, pp. 1033–1038, June 1995.

[9] H. Krömer, "Proposed negative-mass microwave amplifier," *Phys. Rev.*, vol. 109, p. 1856, Mar. 1958.

[10] ——, "Negative effective masses in semiconductors," *Progress in Semiconductors*, vol. 4, pp. 1–34, 1960.

[11] V. I. Gavrilenko and Z. F. Krasil'nik, "Negative mass cyclotron resonance maser," *Opt. Quantum Electron.*, vol. 23, pp. S323–S329, 1991.

[12] N. Sano and A. Yoshii, "Impact-ionization model consistent with the band structure of semiconductors," *J. Appl. Phys.*, vol. 77, pp. 2020–2025, Mar. 1995.

[13] E. Kobayashi, C. Hamaguchi, T. Matsuoka, and K. Taniguchi, "Monte Carlo study of hot-electron transport in an In Ga As/In Al As single heterostructure," *IEEE Trans. Electron Devices*, vol. 36, pp. 2353–2360, Oct. 1989.

[14] M. Fischetti, "Monte Carlo simulation of transport in technologically significant semiconductors of the diamond and zinc-blende structures—Part 1: Homogeneous transport," *IEEE Trans. Electron Devices*, vol. 38, pp. 634–649, Mar. 1989.

[15] J. C. Cao, H. C. Liu, and X. L. Lei, "Simulation of negative-effective-mass terahertz oscillators," *J. Appl. Phys.*, vol. 87, pp. 2867–2873, Mar. 2000.

[16] J. C. Cao, H. C. Liu, X. L. Lei, and A. G. U. Perera, "Chaotic dynamics in THz-driven semiconductors with negative effective mass," *Phys. Rev. B*, to be published.

[17] Z. S. Gribnikov and A. N. Korshak, "Ballistic injection of electrons with negative effective masses," *Semiconductors*, vol. 28, pp. 812–816, Aug. 1994.

[18] N. Z. Vagidov, Z. S. Gribnikov, and A. N. Korshak, "Terahertz-range oscillations of the ballistic current of electrons with a negative effective mass," *JETP Lett.*, pp. 38–43, Jan. 1995.

[19] ——, "Space charge of injected ballistic electrons with negative effective mass," *Semiconductors*, vol. 29, pp. 1014–1020, Nov. 1994.

[20] Z. S. Gribnikov, A. N. Korshak, and N. Z. Vagidov, "Terahertz ballistic current oscillations for carriers with negative effective mass," *J. Appl. Phys.*, vol. 80, pp. 5799–5808, Nov. 1996.

[21] M. I. D'yakonov and A. V. Khaetskii, "Size quantization of holes in semiconductor with complicate valence band and carriers in zero-bandgap semiconductor," *Sov. Phys. JETP*, vol. 55, pp. 917–921, May 1982.

[22] Z. N. Sokolova, V. B. Khalfin, and A. L. Efros, "Size quantization of holes and properties of exciton spectra in quantum well of finite depth," *Sov. Phys. Semicond.*, vol. 22, pp. 1342–1346, Dec. 1989.

[23] L. C. Andreani, A. Pasquarello, and F. Bassani, "Hole subbands in strained Ga As–$Ga_{1-x}Al_xAs$ quantum wells: Exact solution of the effective mass equation," *Phys. Rev. B*, vol. 36, pp. 5887–5894, Oct. 1987.

[24] E. C. Valadares, "Strong anisotropy of hole subbands in (311) Ga As–Al As quantum wells," *Phys. Rev. B*, vol. 46, pp. 3935–3939, Aug. 1992.

[25] R. K. Hayden, D. K. Maude, L. Eaves, E. C. Valadares, M. Henini, F. M. Sheard, O. H. Hughes, J. C. Portal, and L. Cury, "Probing the hole dispersion curves of a quantum well using resonant magnetotunneling spectroscopy," *Phys. Rev. Lett.*, vol. 66, pp. 1749–1752, Apr. 1991.

[26] R. K. Hayden, M. Henini, L. Eaves, D. K. Maude, J. C. Portal, L. Cury, and G. Hill, "Measurement of the anisotropy of the hole dispersion curves in an Al As/Ga As/Al As quantum well grown on a (311) A oriented substrate," *Semicond. Sci. Technol.*, vol. 7, pp. 1080–1084, 1992.

[27] R. K. Hayden, L. Eaves, M. Henini, E. C. Valadares, O. Kuhn, D. K. Maude, J. C. Portal, T. Takamasu, N. Miura, and U. Ekenberg, "Probing the anisotropic dispersion of hole states in (100) and (311) A Al As/ Ga As/Al As quantum wells," *Semicond. Sci. Technol.*, vol. 9, pp. 298–309, 1994.

[28] M. Henini, P. J. Rodgers, P. A. Crump, and B. L. Gallaher, "Growth and electrical transport properties of very high mobility two-dimensional hole gases displaying persistent photoconductivity," *Appl. Phys. Lett.*, vol. 65, pp. 2054–2056, Oct. 1994.

[29] J. J. Heremans, M. B. Santos, and M. Shayegan, "Observation of magnetic focusing in two-dimensional hole systems," *Appl. Phys. Lett.*, vol. 61, pp. 1652–1654, Oct. 1992.

[30] A. G. Davies, R. Newbury, M. Pepper, J. E. F. Frost, D. A. Ritchie, and G. A. C. Jones, "Fractional quantum Hall effect in high-mobility two-dimensional hole gases in titled magnetic fields," *Phys. Rev. B*, vol. 44, pp. 13 128–1331, Nov. 1991.

[31] J. J. Heremans, M. B. Santos, K. Hirakawa, and M. Shayegan, "Mobility anisotropy of two-dimensional hole systems in (311) A Ga As/$Al_xGa_{1-x}As$ heterojunctions," *J. Appl. Phys.*, vol. 76, pp. 1980–1982, Aug. 1994.

[32] B. E. Cole, J. M. Chamberlain, M. Henini, T. Cheng, W. Batty, A. Wittlin, J. A. A. J. Perenboom, A. Ardavan, A. Polisski, and J. Singleton, "Cyclotron resonance in ultra-low-hole-density narrow p-type Ga As/(Al,Ga)As quantum wells," *Phys. Rev. B*, vol. 55, pp. 2503–2511, Jan. 1997.

[33] B. R. Perkins, J. Liu, A. Zaslavsky, Z. S. Gribnikov, V. V. Mitin, E. P. De Poortere, and M. Shayegan, "Nonlinear transport in ballistic semiconductor diodes with negative effective mass carriers," in *Proc. 11 Int. Symp. Space Terahertz Technol.*, Ann Arbor, MI, May 1–3, 2000, pp. 582–589.

[34] I. S. Millard, N. K. Patel, M. Y. Simmons, E. H. Linfield, D. A. Ritchie, G. A. C. Jones, and M. Pepper, "Compressivity studies of double electron and double hole gas systems," *Appl. Phys. Lett.*, vol. 68, pp. 3323–3325, June 1996.

[35] A. R. Hamilton, M. Y. Simmons, F. M. Bolton, N. K. Patel, I. S. Millard, J. T. Nichols, D. A. Ritchie, and M. Pepper, "Fractional quantum Hall effect in bilayer two-dimensional hole systems," *Phys. Rev. B*, vol. 54, pp. R5259–R5262, Aug. 1996.

[36] Z. S. Gribnikov, A. N. Korshak, and V. V. Mitin, "Generation of terahertz electric oscillations by ballistic quantized holes with negative effective mass," *Int. J. Infra. Millimeter Waves*, vol. 20, pp. 213–237, Feb. 1999.

[37] R. R. Bashirov, Z. S. Gribnikov, N. Z. Vagidov, and V. V. Mitin, "Two mechanisms of the negative-effective-mass instability in p-type quantum well-based ballistic $p^+pp^+$-diodes: Simulations with a load," *Appl. Phys. Lett.*, vol. 77, pp. 3785–3787, Dec. 2000.

[38] M. Heiblom, K. Seo, H. P. Meier, and T. W. Hickmott, "Observation of ballistic holes," *Phys. Rev. Lett.*, vol. 60, pp. 828–831, Feb. 1988.

[39] Z. S. Gribnikov, N. Z. Vagidov, and V. V. Mitin, "Two-stream instability and oscillatory regimes induced in ballistic diodes and field-effect transistors," *J. Appl. Phys.*, vol. 88, pp. 6736–6745, Dec. 2000.

[40] Z. S. Gribnikov, "Negative differential conductivity in a multilayer heterostructure," *Sov. Phys. Semicond.*, vol. 6, pp. 1204–1205, Jan. 1973.

[41] Z. S. Gribnikov, K. Hess, and G. A. Kosinovsky, "Nonlocal and nonlinear transport in semiconductors: Real-space transfer effects," *J. Appl. Phys.*, vol. 77, pp. 1337–1373, Feb. 1995.

[42] L. Pfeiffer, K. W. West, H. L. Störmer, J. P. Eisenstein, K. W. Baldwin, D. Gershoni, and J. Spector, "Formation of high quality two-dimensional electron gas on cleaved GaAs," *Appl. Phys. Lett.*, vol. 56, pp. 1697–1699, Apr. 1990.

[43] H. L. Störmer, L. N. Pfeiffer, K. W. Baldwin, K. W. West, and J. Spector, "Atomically precise superlattice potential imposed on a two-dimensional electron gas," *Appl. Phys. Lett.*, vol. 58, pp. 726–728, Febr. 1991.

[44] L. Pfeiffer, H. L. Störmer, K. W. Baldwin, K. W. West, A. R. Goñi, A. Pinczuk, R. C. Ashoori, M. M. Dignam, and W. Wegschneider, "Cleaved edge overgrowth for quantum wire fabrication," *J. Cryst. Growth*, vol. 127, pp. 849–857, 1993.

[45] A. Yacoby, H. L. Störmer, N. S. Wingreen, L. N. Pfeiffer, K. W. Baldwin, and K. W. West, "Nonuniversal conductance quantization in quantum wire," *Phys. Rev. Lett.*, vol. 77, pp. 4612–4615, Nov. 1996.

[46] A. Majumdar, L. P. Rokhinson, D. C. Tsui, L. N. Pfeiffer, and K. W. West, "Effective mass enhancement of two-dimensional electrons in a one-dimensional superlattice potential," *Appl. Phys. Lett.*, vol. 76, pp. 3600–3602, June 2000.

[47] M. Yoshita, H. Akijama, T. Someya, and H. Sakaki, "Microphotoluminescence characterization of cleaved edge overgrowth T-shaped $In_xGa_{1-x}As$ quantum wires," *J. Appl. Phys.*, vol. 83, pp. 3777–3783, Apr. 1998.

**Zinovi S. Gribnikov** was born in Kiev, Ukraine. He received the engineer-physicist degree from Kiev Politechnical Institute, Ukraine, the Ph.D. degree in physics and mathematics from P.N. Lebedev Physics Institute, Moscow, Russia, and the doctor of physics and mathematics degree from the Semiconductor Physics Institute, Ukrainian National Academy of Sciences, Ukraine.

He was a Senior Scientist and Head of the Semiconductor Device Theory Laboratory in the Semiconductor Physics Institute. He is currently with the Department of Electrical and Computer Engineering, Wayne State University, Detroit, MI, and the Department of Electrical Engineering and Computer Science at the University of Michigan, Ann Arbor. He is an author and coauthor of more than 190 papers (including monographs and monograph reviews).

**Rustam R. Bashirov** was born in Kazan, Russia. He received the B.Sc. degree in physics from Daghestan State University, Makhachkala, Russia, in 1976.

He is currently with the Department of Electrical and Computer Engineering, Wayne State University, Detroit, MI.

**Vladimir V. Mitin** (M'89–SM'94) received the M.Sc. degree in radiophysics from Rostov State University, Rostov, Russia, in 1968 and the Ph.D. degree in physics from the Institute of Semiconductor Physics, National Academy of Sciences, Kiev, Ukraine, in 1971.

Since 1989, he has been with the Department of Electrical and Computer Engineering, Wayne State University (WSU), Detroit, MI, where he is currently a Professor. He is the author of more than 350 professional publications. He has graduated 11 Ph.D. students and four master's students at WSU.

Dr. Mitlin is a Senior Member of the IEEE Electron Devices Society.